

RESEARCH ARTICLE

Radiation degradation characteristics of component subcells in inverted metamorphic triple-junction solar cells irradiated with electrons and protons

Mitsuru Imaizumi^{1*}, Tetsuya Nakamura¹, Tatsuya Takamoto², Takeshi Ohshima³ and Michio Tajima⁴

¹ Japan Aerospace Exploration Agency, 2-1-1 Sengen, Tsukuba, Ibaraki 305-8505, Japan

² SHARP Corporation, 492 Minosyo, Yamatokoriyama, Nara 639-2198, Japan

³ National Institutes for Quantum and Radiological Science and Technology, 1233 Watanuki, Takasaki, Gunma 370-1292, Japan

⁴ Japan Aerospace Exploration Agency, 3-1-1 Yoshinodai, Chuou, Sagami-hara, Kanagawa 252-5210, Japan

ABSTRACT

The radiation response of $\text{In}_{0.5}\text{Ga}_{0.5}\text{P}$, GaAs, $\text{In}_{0.2}\text{Ga}_{0.8}\text{As}$, and $\text{In}_{0.3}\text{Ga}_{0.7}\text{As}$ single-junction solar cells, whose materials are also used as component subcells of inverted metamorphic triple-junction (IMM3J) solar cells, was investigated. All four types of cells were prepared using a simple device layout and irradiated with high-energy electrons and protons. The essential solar cell characteristics, namely, light-illuminated current–voltage (LIV), dark current–voltage (DIV), external quantum efficiency (EQE), and two-dimensional photoluminescence (2D-PL) imaging were obtained before and after irradiation, and the corresponding changes due to the irradiations were compared and analyzed. The degradation of the cell output parameters by electrons and protons were plotted as a function of the displacement damage dose. It was found that the radiation resistance of the two InGaAs cells is approximately equivalent to that of the InGaP and GaAs cells from the materials standpoint, which is a result of different initial material qualities. However, the InGaAs cells show relatively low radiation resistance to electrons especially for the short-circuit current (I_{sc}). By comparing the degradation of I_{sc} and EQE, data, it was confirmed that the greater decrease of minority-carrier diffusion length in InGaAs compared with InGaP and GaAs causes severe degradation in the photo-generation current of the InGaAs bottom subcells in IMM3J structures. Additionally, it was found that the InGaP and two InGaAs cells exhibited equivalent radiation resistance of V_{oc} , but radiation response mechanisms of V_{oc} are thought to be different. Further analytical studies are necessary to interpret the observed radiation response of the cells. © 2016 The Authors. *Progress in Photovoltaics: Research and Applications* published by John Wiley & Sons Ltd.

KEYWORDS

space solar cell; IMM; InGaP; GaAs; InGaAs; radiation degradation; proton; electron

*Correspondence

Mitsuru Imaizumi, Tsukuba Space Center, Japan Aerospace Exploration Agency, 2-1-1 Sengen, Tsukuba, Ibaraki 305-8505, Japan.

E-mail: imaizumi.mitsuru@jaxa.jp

Received 27 July 2015; Revised 25 September 2016; Accepted 29 September 2016

This is an open access article under the terms of the Creative Commons Attribution-NonCommercial License, which permits use, distribution and reproduction in any medium, provided the original work is properly cited and is not used for commercial purposes.

1. INTRODUCTION

At present, the inverted metamorphic (IMM) multi-junction (MJ) solar cells formed of $\text{In}_{0.5}\text{Ga}_{0.5}\text{P}/\text{GaAs}/\text{In}_x\text{Ga}_{1-x}\text{As}$ material system have received considerable attention and are being developed as next-generation space solar cells [1–5] owing to their higher conversion efficiency compared with the currently used conventional

$\text{In}_{0.5}\text{Ga}_{0.5}\text{P}/\text{GaAs}/\text{Ge}$ triple-junction space solar cells [6,7]. In addition, the IMM-MJ cells are essentially light-weight thin film cells, because the semiconductor layers constituting the solar cell structure are inversely grown on the substrates, which are subsequently removed during the device fabrication process. This enables great weight reduction of the solar cells and consequently the increase in the specific power on spacecraft power panels.

Furthermore, the thin structure of these cells offer the advantage of flexibility, facilitating the development of thin and flexible solar array sheets [8–10] that could potentially be mounted on non-flat surfaces of spacecraft. Thus, the high-efficiency, lightweight, and flexible properties of IMM-MJ cells provide great advantages for space applications.

To design an MJ solar cell for space applications, one has to understand the radiation degradation characteristics of each subcell in a designated MJ structure. In the design consideration of $\text{In}_{0.5}\text{Ga}_{0.5}\text{P}/\text{GaAs}/\text{In}_x\text{Ga}_{1-x}\text{As}$ IMM triple-junction (IMM3J) space cells, the degradation characteristics of the top InGaP and middle GaAs subcells are already well understood because they are adopted in the current $\text{In}_{0.5}\text{Ga}_{0.5}\text{P}/\text{GaAs}/\text{Ge}$ triple-junction (3J) design for space cells [11]. On the other hand, for the bottom $\text{In}_x\text{Ga}_{1-x}\text{As}$ subcells with indium concentration (x) higher than 10%, the radiation degradation behavior has not yet been sufficiently clarified because the material is relatively new for space solar cell application [12,13]. In addition, the InGaAs subcells in the IMM3J cells are lattice-mismatched to the InGaP/GaAs system. Although lattice-mismatch relaxing buffer layers are inserted between the GaAs middle cell layer and the InGaAs bottom cell layer [14,15], the InGaAs cells should incorporate a certain density of defects including misfit dislocations and internal strain. Therefore, it is highly important to investigate the radiation resistance of InGaAs cells grown on lattice-mismatched GaAs or Ge substrates. The same structures of the top InGaP and middle GaAs subcells in the current space 3J can be fundamentally applied to the space IMM3J cells. Practically, several types of IMM-MJ space solar cells have been developed on the basis of the knowledge from the present space 3J cells [1–5]. However, additional modification and improvement of the structure becomes possible once further knowledge on radiation degradation characteristics of such lattice-mismatched InGaAs cells is gained.

In this study, we compare the effects of radiation on the output characteristics of two types of $\text{In}_x\text{Ga}_{1-x}\text{As}$ single-junction (1J) solar cells with those of $\text{In}_{0.5}\text{Ga}_{0.5}\text{P}$ and GaAs 1J solar cells. For each solar cell structure we prepared a number of samples in order to analyze the degradation behavior and relative radiation resistance for irradiation with either high-energy protons or electrons. We note that we adopt a very simple device structure for the sample cells in this study. This is because the purpose of this study is not to optimize the subcell structure for the InGaP/GaAs/InGaAs IMM3J cells but to reveal the radiation degradation characteristics of the three cells and compare the radiation resistance of the 1J cells from the view point of material properties.

2. EXPERIMENTAL

Four types of 1J solar cells, namely, $\text{In}_{0.5}\text{Ga}_{0.5}\text{P}$, GaAs, and two $\text{In}_x\text{Ga}_{1-x}\text{As}$ cells with indium content x of 0.2 and 0.3, whose materials are typically used for component

subcells in IMM3J cells, were prepared for this study. The cell layers were grown onto GaAs (100) substrates by metal–organic vapor phase epitaxy. Figure 1 illustrates the layer structure of the sample solar cells. The base-layer thickness of the InGaP cell is $1.0\ \mu\text{m}$, which is thicker than the InGaP top-cell in current space 3J cells, whereas that of

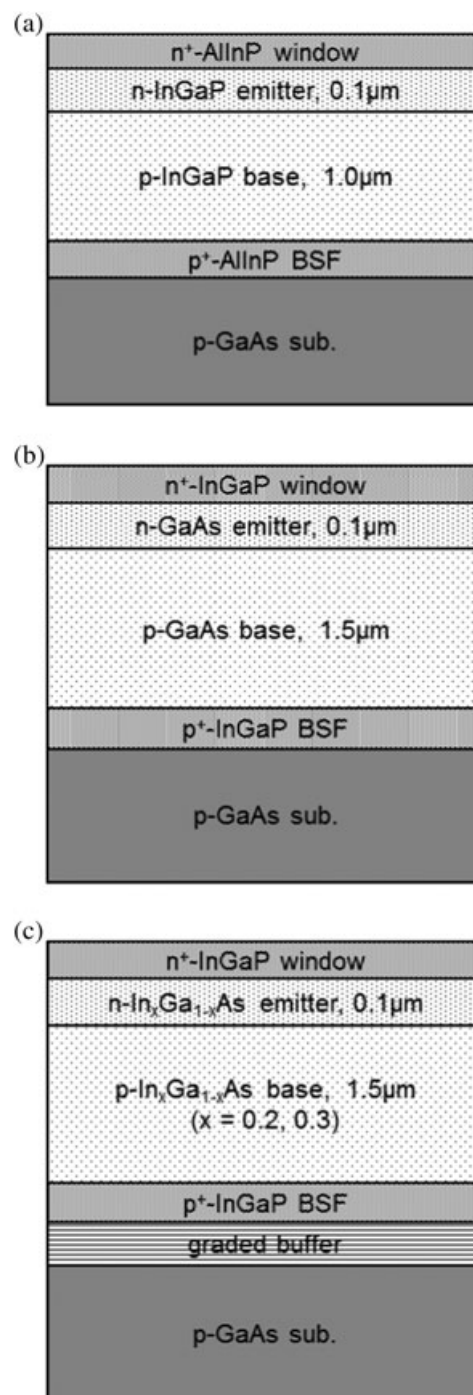


Figure 1. Layered structure of the four types of solar cells analyzed in this study. (a) InGaP cell, (b) GaAs cell, and (c) InGaAs cells.

Table I. Average I_{sc} , V_{oc} , and P_{max} values of the representative $In_{0.5}Ga_{0.5}P$, GaAs, $In_{0.2}Ga_{0.8}As$, and $In_{0.3}Ga_{0.7}As$ 1 J solar cells (without antireflective coating).

Parameter	$In_{0.5}Ga_{0.5}P$ cell	GaAs cell	$In_{0.2}Ga_{0.8}As$ cell	$In_{0.3}Ga_{0.7}As$ cell
# of cells	101	102	99	103
I_{sc} (mA/cm ²)	13.35 (0.143)	22.26 (0.122)	28.45 (0.238)	30.48 (0.417)
V_{oc} (V)	1.426 (0.005)	1.057 (0.005)	0.695 (0.010)	0.548 (0.005)
W_{oc} (V)*1	0.42	0.36	0.43	0.44
P_{max} (mW/cm ²)	15.56 (0.364)	18.82 (0.363)	14.94 (0.525)	12.24 (0.443)

The values in parentheses are the standard deviations.
 *1Bandgaps are estimated from external quantum efficiency absorption edges.

the GaAs and the InGaAs cells is 1.5 μm , which is equivalent to or thinner than that of the GaAs middle and InGaAs bottom subcells in typical space 3J cells. The reason for selecting such thicknesses of the base layers is to easily observe and compare the effect of the decrease in minority-carrier diffusion length because of radiation on the cell performance. The two InGaAs cells were grown on the GaAs substrate after growing step-graded InGaP buffer layers, which are commonly used for growth of IMM3J cells. Therefore, the crystal quality of the metamorphic

InGaAs layers is considered to be equivalent to that in IMM3J cells. The size of the cells is 10 \times 10 mm. An anti-reflection coating was not applied in order to avoid the influence of inhomogeneity of reflectance between the samples. The current–voltage (I–V) characteristics under simulated solar light (LIV), I–V characteristics in dark (DIV), and the external quantum efficiency (EQE) measurements were performed at JAXA Tsukuba Space Center before and after the irradiation tests to be described later. The LIV measurements were performed under the standard condition (AM0, 1sun = 136.7 mW/cm², 25 °C) [16] using a dual-light-source solar simulator (WACOM WXS-130S-L2HV), from which the solar cell output parameters, that is, the short-circuit current (I_{sc}), the open-circuit voltage (V_{oc}), and the maximum power (P_{max}) were determined. The average values of the three output parameters for the four types of cells are summarized in Table I.

The two-dimensional photoluminescence (2D-PL) image [17] was recorded at the Institute of Space and Astronautical Science at JAXA. The plan-view PL image of the entire cell was recorded with a precise x – y stage using focused excitation lasers (488 nm for the InGaP cells and 532 nm for the GaAs and InGaAs cells). The data collection pitch, which is equivalent to the image resolution, was 20 μm . The PL intensity of the images before and after the irradiations was calibrated using reference cells, which were not irradiated.

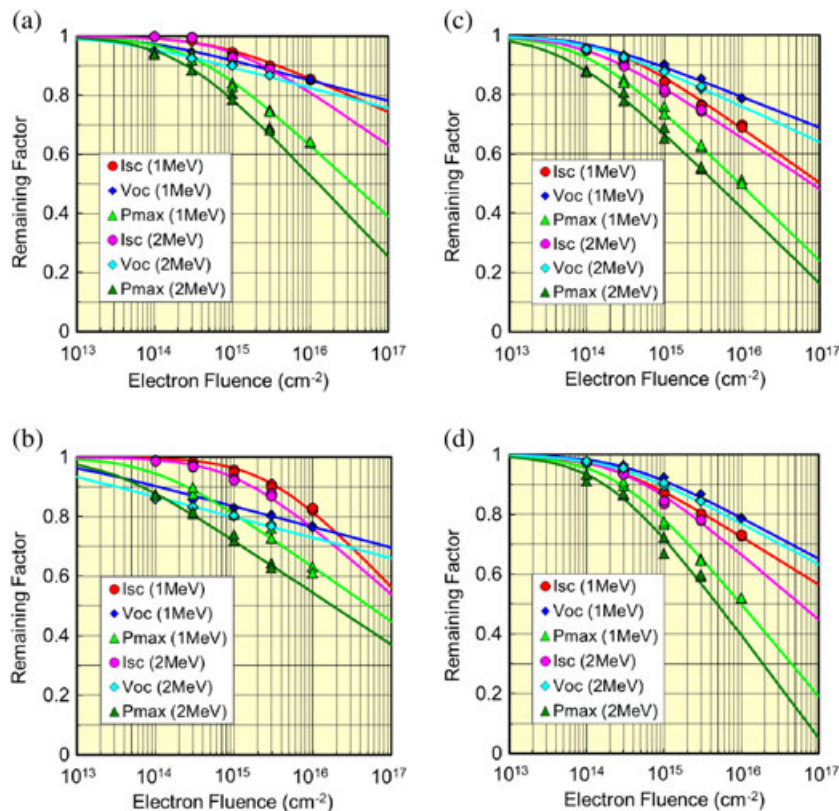


Figure 2. Degradation characteristics of I_{sc} , V_{oc} , and P_{max} as a result of electron irradiations. (a) InGaP cell, (b) GaAs cell, (c) $In_{0.2}Ga_{0.8}As$ cell, and (d) $In_{0.3}Ga_{0.7}As$ cell.

The four types of 1J cells considered in this study were subjected to irradiation tests using electrons and protons of various energies. Two cells from each type of cell were irradiated for each irradiation condition (particle, energy, and fluence) to confirm reproducibility. Electrons of energy 1 and 2 MeV and protons of energy 3 MeV pass through the cell structures with minimal slow down, and thus, the radiation defects are created uniformly throughout the cell. According to SRIM transport simulations [18], protons of energy 200 and 380 keV also pass through the cell, but the lower energy protons create a greater number of defects than the 3 MeV protons, especially in the rear of the cells. All irradiation tests were carried out at the Japan Atomic Energy Agency in Takasaki, Japan [19]. The LIV, DIV, EQE, and 2D-PL images were recorded before and after the irradiation tests.

3. RESULTS

The results of the electron and proton irradiations are shown in Figures 2 and 3, respectively. Each figure reveals the degradation of I_{sc} , V_{oc} , and P_{max} of the (a) InGaP, (b) GaAs, (c) $In_{0.2}Ga_{0.8}As$, and (d) $In_{0.3}Ga_{0.7}As$ 1J cells derived from their LIV characteristics before and after the electron and proton irradiations. The degradations of the aforementioned three output parameters are expressed as

remaining factor (the ratio of degraded value to initial value) as a function of the particle fluence. The degradation characteristic curves, indicated with solid lines in the figures, were obtained by fitting the data using the following equation [20]:

$$\frac{X}{X_0} = 1 - A \log \left(1 + \frac{\phi}{\phi_0} \right) \quad (1)$$

where X and X_0 are the output parameter values before and after irradiation, ϕ is the fluence, and A and ϕ_0 are the fitting parameters.

In the case of electron irradiation, higher energy electrons induce greater radiation damage, whereas in the case of proton irradiation, the opposite is observed. The degradation tendencies of all three output parameters of all four types of cells indicated in Figures 2 and 3 follow a similar trend. It should be mentioned that the fill factor of all four cells in both cases of electron and proton irradiations follows the same degradation trend as observed for I_{sc} .

Figures 4 and 5 depict the changes in LIV and EQE of (a) InGaP, (b) GaAs, (c) $In_{0.2}Ga_{0.8}As$, and (d) $In_{0.3}Ga_{0.7}As$ 1J cells as a result of the irradiation of 1 MeV electrons and 3 MeV protons irradiations, respectively. In all cases, the EQE in the longer wavelength region, which represents light absorption in the deep inside the cells, showed significant degradations. On the other hand, the EQE in the shorter wavelength region, corresponding to light

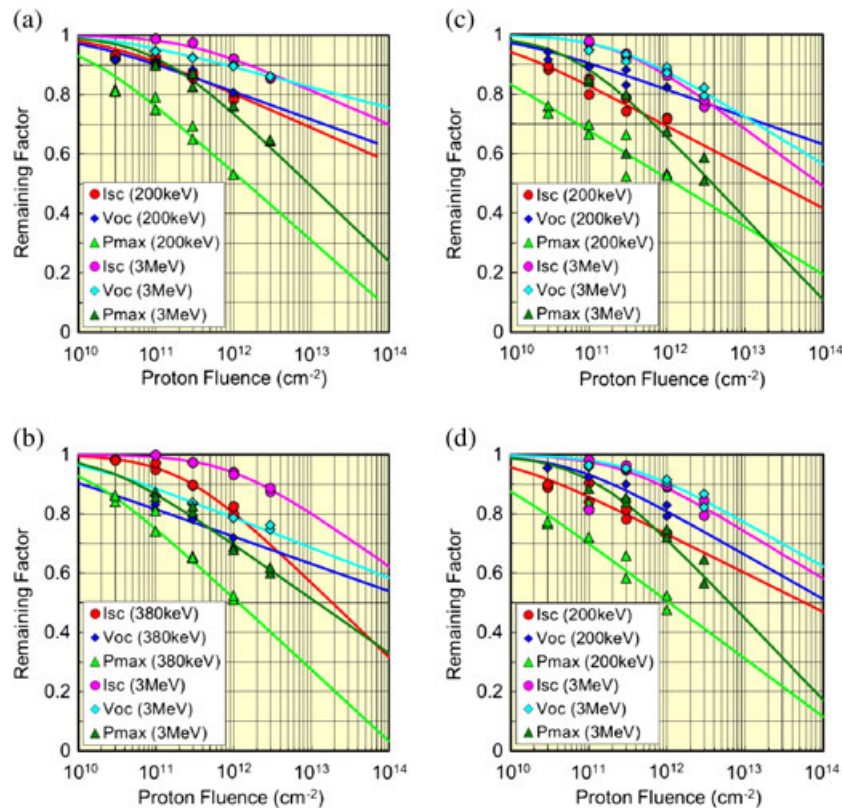


Figure 3. Degradation characteristics of I_{sc} , V_{oc} , and P_{max} as a result of proton irradiations. (a) InGaP cell, (b) GaAs cell, (c) $In_{0.2}Ga_{0.8}As$ cell, and (d) $In_{0.3}Ga_{0.7}As$ cell.

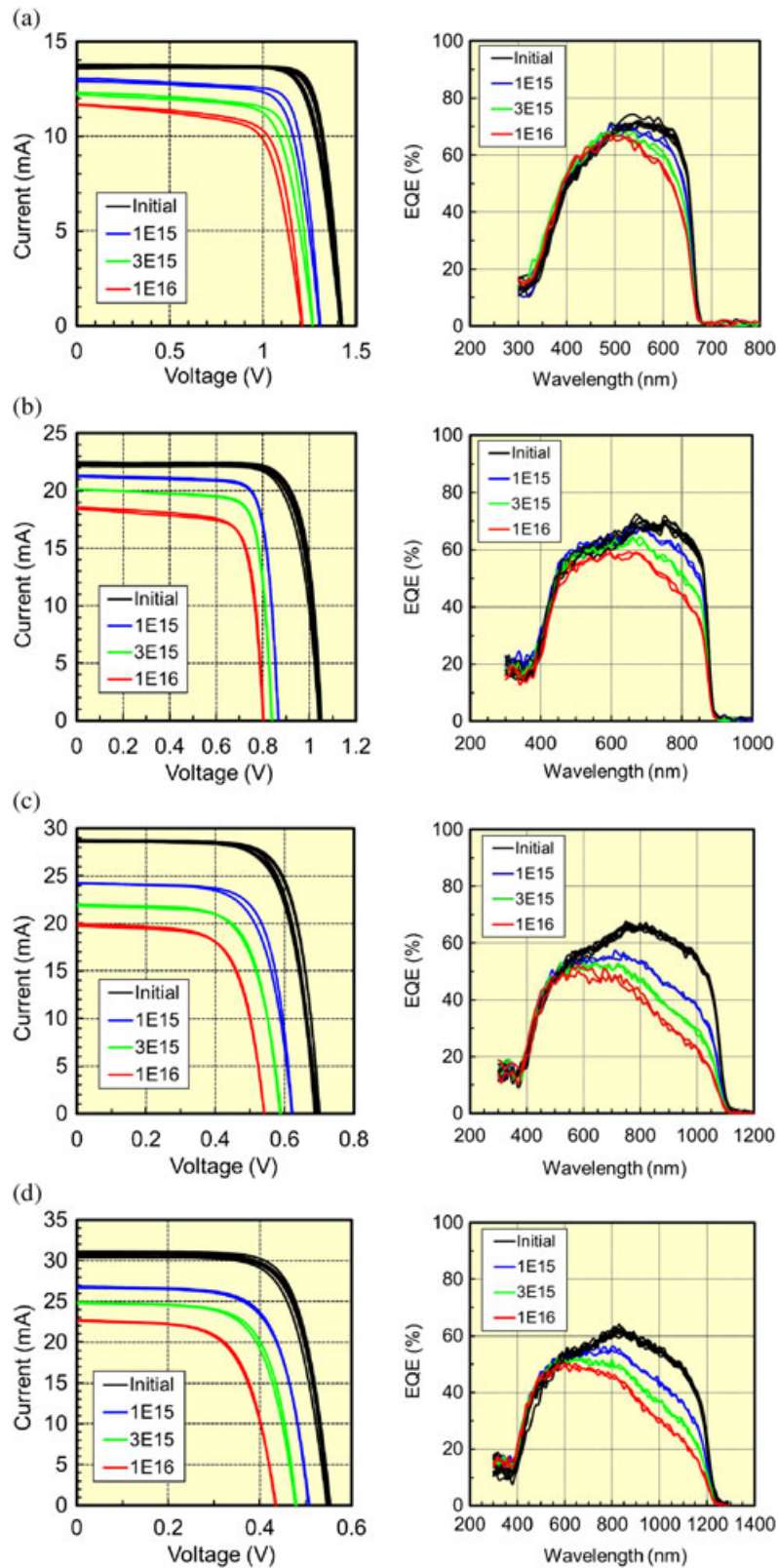


Figure 4. Change in light current–voltage curves (LIV) and external quantum efficiency (EQE) as a result of 1 MeV electron irradiations. The number in legend is fluence. (For instance, 1E15 means $1 \times 10^{15} \text{ cm}^{-2}$.) (a) InGaP cell, (b) GaAs cell, (c) $\text{In}_{0.2}\text{Ga}_{0.8}\text{As}$ cell, and (d) $\text{In}_{0.3}\text{Ga}_{0.7}\text{As}$ cell.

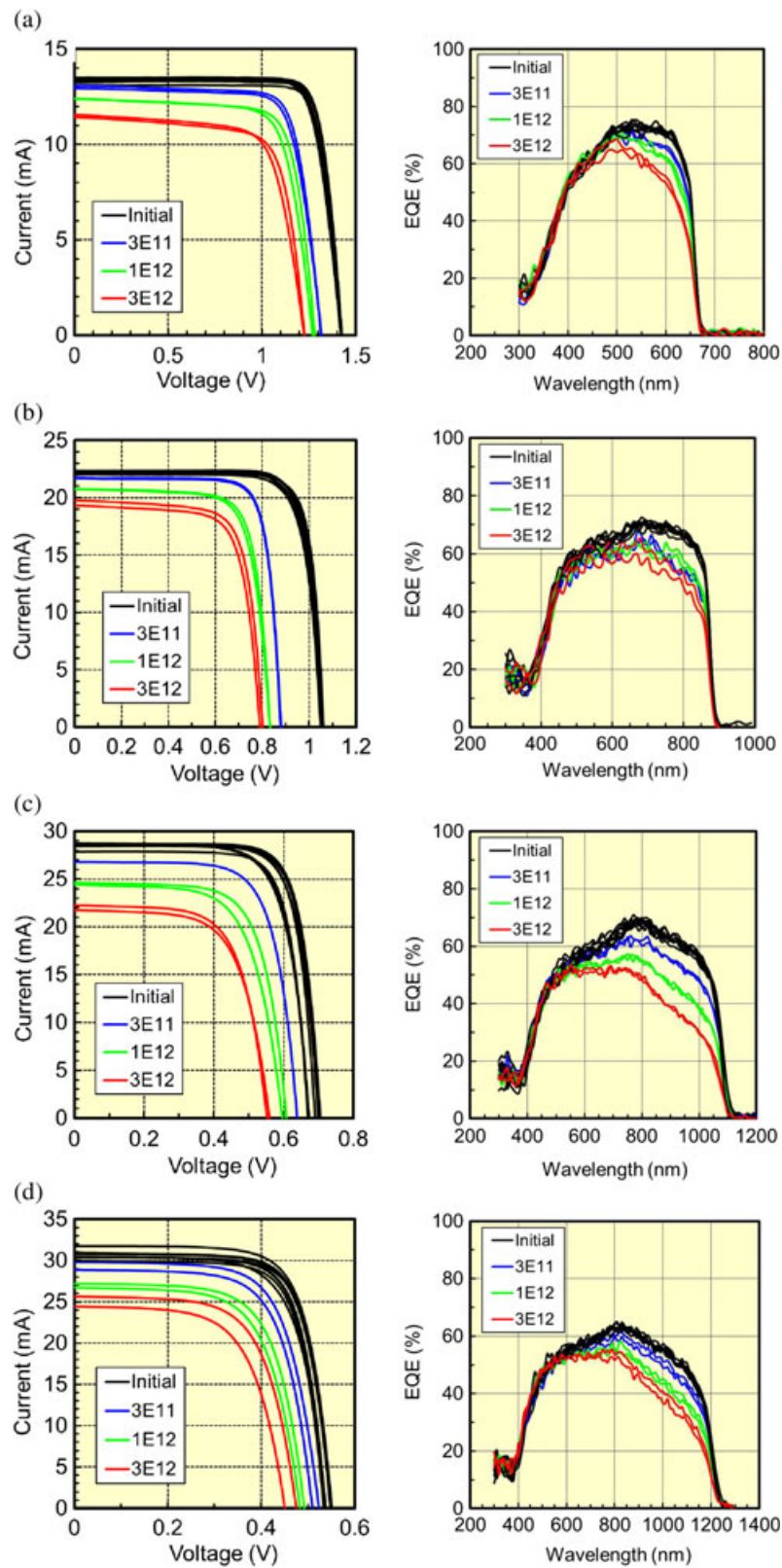


Figure 5. Change in light current–voltage curves (LIV) and external quantum efficiency (EQE) as a result of 3 MeV proton irradiations. The number in the legend is the fluence. (For instance, 3E11 means $3 \times 10^{11} \text{ cm}^{-2}$.) (a) InGaP cell, (b) GaAs cell, (c) $\text{In}_{0.2}\text{Ga}_{0.8}\text{As}$ cell, and (d) $\text{In}_{0.3}\text{Ga}_{0.7}\text{As}$ cell.

absorption in shallower regions, does not show apparent degradation. A similar trend was also confirmed in the results of 200/380 keV proton and 2 MeV electron irradiations. This fact indicates that the degradation in EQE observed in all four types of cells was principally caused by the decrease in minority-carrier diffusion length. In addition, the EQE degradation implies that the irradiations did not induce substantial increase of the front-surface carrier recombination velocity [21].

Figures 6 and 7 depict the DIV curves of (a) InGaP, (b) GaAs, (c) $\text{In}_{0.2}\text{Ga}_{0.8}\text{As}$, and (d) $\text{In}_{0.3}\text{Ga}_{0.7}\text{As}$ 1J cells before and after 1 MeV electron and 3 MeV proton irradiations. Only the curves of one of the two cells under each irradiation condition are shown in the figures. The black lines correspond to the “initial” results obtained before the irradiation of the cells. As can be seen, some cells (for example, (b) in Figure 6 and (d) in Figure 7) show considerable dispersion. However, after irradiation, the dark current increases with fluence for most of the cells. Accordingly, it is considered that the dispersion in the initial DIV characteristics is unlikely to influence the results.

The diode factor (n) and the reverse saturation current (I_0) were determined by fitting the DIV characteristics using the simple one-diode model without series/parallel resistance. Some cells showed high current in the low-voltage region, which cannot be fitted using this model.

This may be attributed to extrinsic effects, such as cell edge leakage current, and hence, this was ignored in the fitting process for these samples. In other samples, the simple model fitted well.

Figure 8(a) and (b) shows the representative 2D-PL images of the four kinds of 1J cells before and after 1 MeV electron irradiation with fluence of $3 \times 10^{15} \text{ cm}^{-2}$ and 3 MeV proton irradiation with fluence of $3 \times 10^{12} \text{ cm}^{-2}$, respectively. The intensity contrast was adjusted by comparing the corresponding images of the non-irradiated reference cells of each type taken at the same time. This normalization procedure is required because the absolute values of the PL intensity were not always reproducible because exactly the same setting of the optical devices between the excitation laser and the samples was not possible. The images of the two InGaAs cells clearly display the grid electrode. This is attributed to the scattering of the excitation laser light because the band-pass filter used for the 2D-PL observation of the InGaAs cells passes the wavelength of $2 \times 532 \text{ nm}$ (second-order harmonic).

The PL is considered to be emitted from the surface n^+ -type emitter layers and space charge regions, that is, the top part of the p-base layers because the excitation light is absorbed mostly within a micron from the cell surface. In addition, the PL from the n^+ -type emitter layer should be dominant because the carrier concentration of the emitter

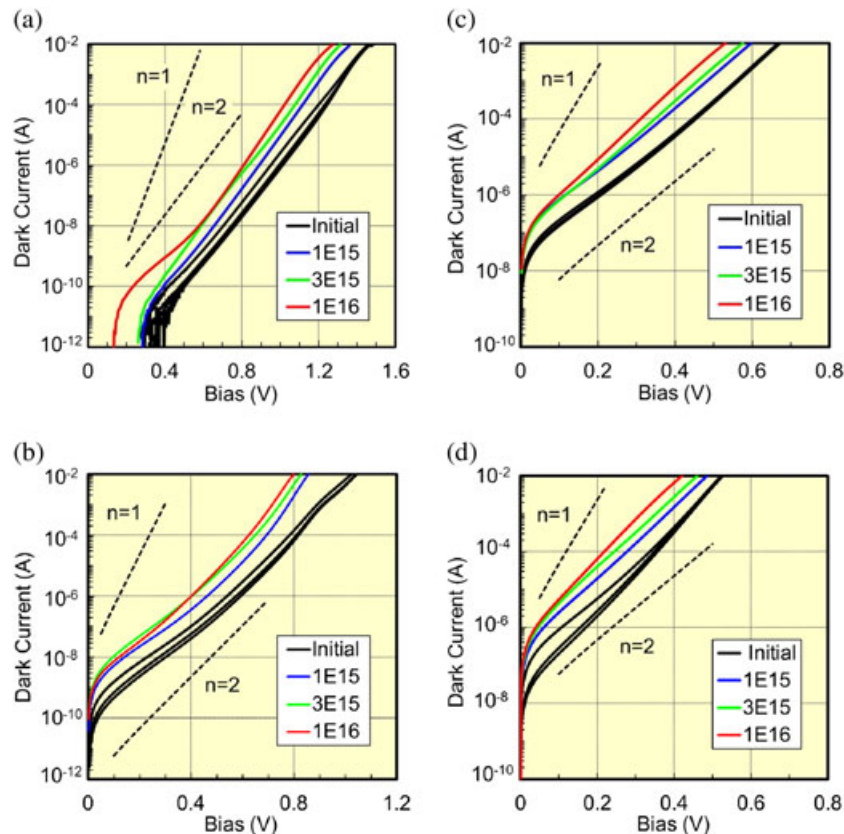


Figure 6. Change in dark current–voltage (DIV) characteristics as a result of 1 MeV electron irradiations. The number in the legend is the fluence. (For instance, 1E15 means $1 \times 10^{15} \text{ cm}^{-2}$.) (a) InGaP cell, (b) GaAs cell, (c) $\text{In}_{0.2}\text{Ga}_{0.8}\text{As}$ cell, and (d) $\text{In}_{0.3}\text{Ga}_{0.7}\text{As}$ cell.

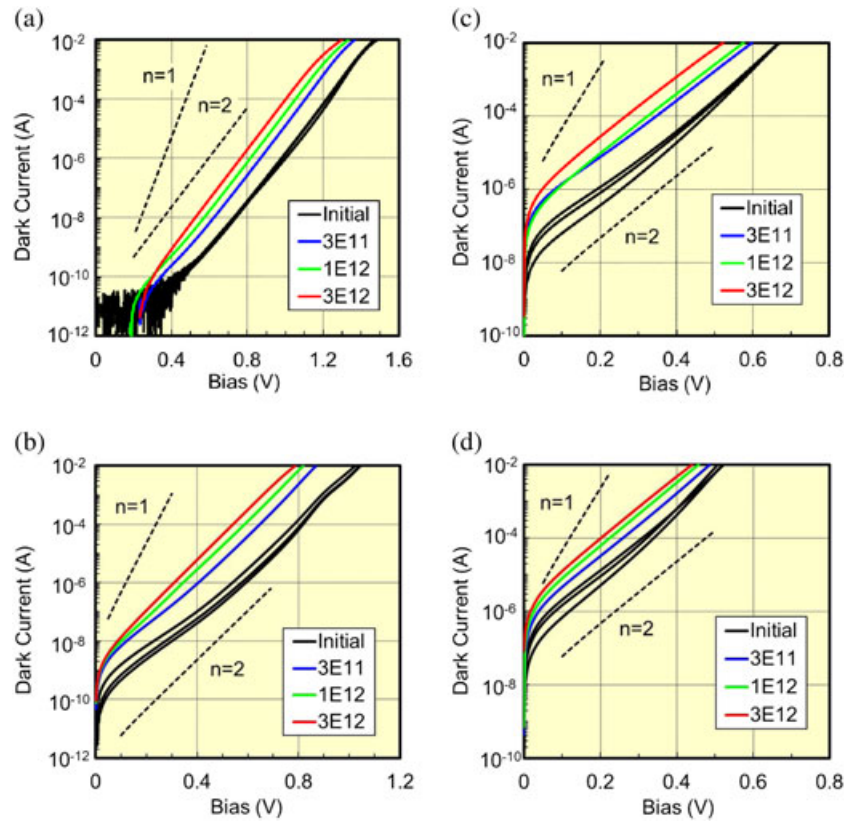


Figure 7. Change in current–voltage characteristics in dark (DIV) as a result of 3 MeV proton irradiations. The number in the legend is the fluence. (For instance, 3E11 means $3 \times 10^{11} \text{ cm}^{-2}$.) (a) InGaP cell, (b) GaAs cell, (c) $\text{In}_{0.2}\text{Ga}_{0.8}\text{As}$ cell, and (d) $\text{In}_{0.3}\text{Ga}_{0.7}\text{As}$ cell.

layer is more than two orders of magnitude higher than that of the subjacent base layer. Accordingly, the change in intensity is an indication of the damage in the cell surface region. Before irradiation, the observed PL intensity tends to be stronger in the location between the finger electrodes for the InGaP and the GaAs cells, whereas it is quite uniform for the two InGaAs cells. After irradiation, there is a significant reduction in the PL intensity of the InGaP and GaAs cells, whereas negligible change is observed in those of the two InGaAs cells.

4. DISCUSSION

4.1. Degradation characteristics

Table II compares the fluence of 1 MeV electrons with that of 3 MeV protons, both of which inflict equivalent degradation on the output cell parameters (90% I_{sc} , 90% V_{oc} , and 80% P_{max}). These fluences were derived from fitting the degradation curves shown in Figures 2 and 3. The ratio indicates the value for 1 MeV electron fluence divided by the value of the 3 MeV proton fluence and gives the relative resistance of 1 MeV electrons to 3 MeV protons. As can be inferred from the ratios, the InGaAs cells are less resistant to electrons compared with the InGaP and GaAs cells, especially for I_{sc} .

To confirm the relative radiation resistance between the four types of 1J cells, the non-ionizing energy loss values of $\text{In}_{0.5}\text{Ga}_{0.5}\text{P}$, GaAs, $\text{In}_{0.2}\text{Ga}_{0.8}\text{As}$, and $\text{In}_{0.3}\text{Ga}_{0.7}\text{As}$ for both electrons and protons were calculated and the degradation data shown in Figures 2 and 3 were plotted in Figure 9 as a function of the displacement damage dose (DDD), which represents the capability of an energized charged particle to create defects in a material [22]. The threshold energy of recoil used in the non-ionizing energy loss calculation were 7 eV for indium, 10 eV for gallium and arsenic, and 9 eV for phosphorous. The DDD plot enables us to compare the radiation resistance with electrons and protons regardless of their energies. In Figure 9 (a) and (b), we assume that the “n” parameter for electron degradation [23] is unity because the degradation due to 1 and 2 MeV electrons seems to collapse into a single curve for all four types of cells.

In the case of I_{sc} degradation, the InGaAs cells obviously show less radiation resistance than the InGaP and GaAs cells, which agrees with the trend indicated by Table II. The difference in the remaining factor for both electrons and protons is approximately 0.1; this tells us that a greater margin of current output is necessary for InGaAs bottom cells when designing IMM3J structures. On the other hand, the V_{oc} degradation of the GaAs cell exhibits more drastic than that for the InGaP and the two InGaAs cells. However, this is not attributed to a poor GaAs cell

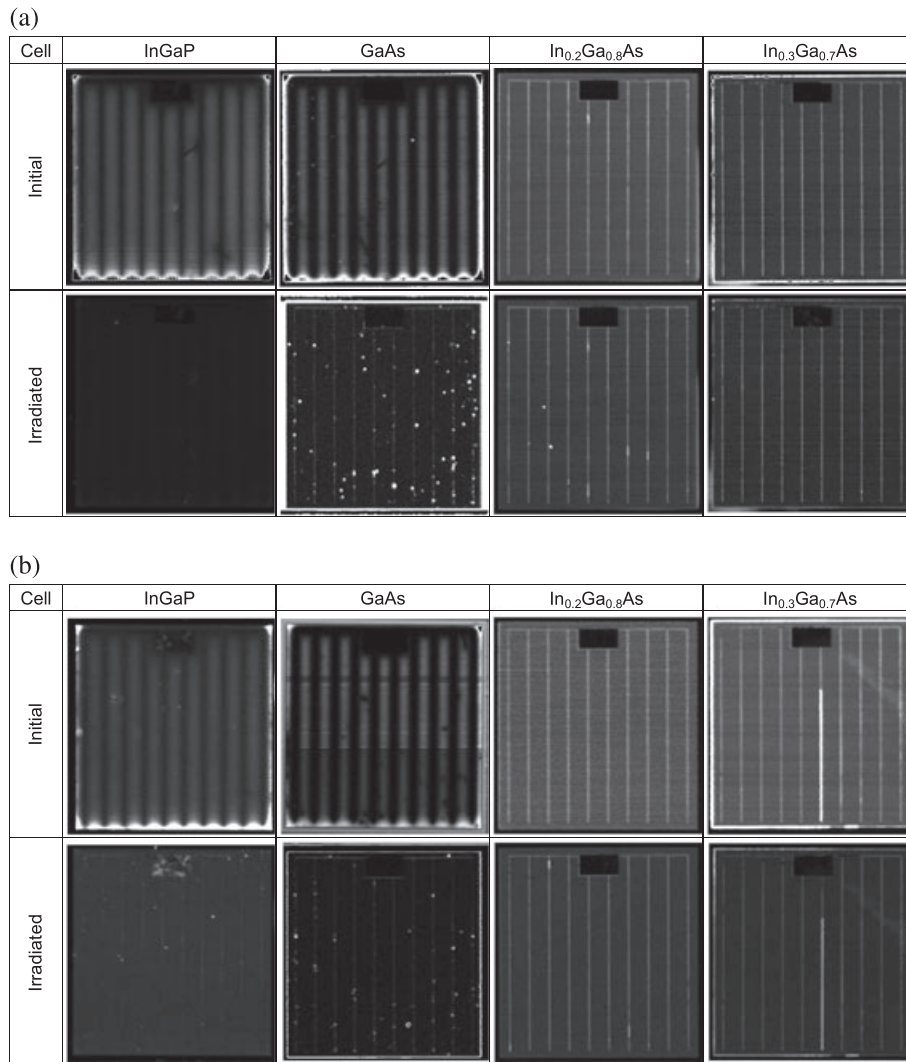


Figure 8. Two-dimensional photoluminescence images before and after 1 MeV electron and 3 MeV proton irradiations. (a) 1 MeV electron, fluence of $3 \times 10^{15} \text{ cm}^{-2}$ and (b) 3 MeV proton, fluence of $3 \times 10^{12} \text{ cm}^{-2}$.

property. In fact, the quality of the GaAs cell is considered to be the highest of the four cell materials before irradiation, because its difference between bandgap and V_{oc} , which is often called W_{oc} , is the smallest (Table I). In general, high initial performance cells show less radiation resistance in terms of the remaining factor. On the contrary, low initial cell performance means that such cells are already “degraded” with respect to their intrinsic counterparts with high performance because of, for example, low-quality material. Therefore, the additional damage upon radiation will not be so effective and thus the degradation appears to be smaller.

4.2. Short-circuit current degradation

To analyze the decrease in I_{sc} as a result of electron and proton irradiations, we calculated the remaining factors of two types of integrated EQE: one for full absorption response and another for partial absorption as occurs for

subcells in an InGaP/GaAs/InGaAs IMM3J cell (from 650/870 nm for the GaAs/InGaAs cells to their absorption edges). For this analysis, we selected 1 MeV electrons with a fluence of $3 \times 10^{15} \text{ cm}^{-2}$ and 3 MeV protons with a fluence of $3 \times 10^{12} \text{ cm}^{-2}$ (cf. Figures 4 and 5) because their damage levels, expressed as DDD values, are approximately the same (Table III). The average remaining factors obtained from integrating the corresponding EQE of the samples for electron and proton irradiations are indicated by the bar graphs in Figure 10(a) and (b) and compared with the remaining factor of I_{sc} .

From the EQE shown in Figures 4 and 5, no change in the short wavelength region can be recognized for any of the four types of cells. As previously noted, the degradation in I_{sc} is principally caused by the decrease in the minority-carrier diffusion length, which is supported by the good agreement between the remaining factors of I_{sc} (red bars) and the integrated EQE indicated as “EQE-Full”

Table II. Fluences of 1 MeV electrons and 3 MeV protons that inflict equivalent degradation on the InGaP, GaAs, In_{0.2}Ga_{0.8}As, and In_{0.3}Ga_{0.7}As 1 J solar cells.

Parameter	Cell	1 MeV		Ratio Φ_e/Φ_p
		electron fluence Φ_e (cm ⁻²)	3 MeV proton fluence Φ_p (cm ⁻²)	
90% I_{sc}	InGaP	3.8×10^{15}	1.6×10^{12}	2380
	GaAs	3.5×10^{15}	2.3×10^{12}	1560
	In _{0.2} Ga _{0.8} As	5.0×10^{14}	5.6×10^{11}	890
	In _{0.3} Ga _{0.7} As	6.4×10^{14}	8.0×10^{11}	800
90% V_{oc}	InGaP	1.9×10^{15}	8.0×10^{11}	2380
	GaAs	1.1×10^{14}	6.7×10^{10}	1640
	In _{0.2} Ga _{0.8} As	8.2×10^{14}	6.4×10^{11}	1280
	In _{0.3} Ga _{0.7} As	1.3×10^{15}	1.1×10^{12}	1180
80% P_{max}	InGaP	1.7×10^{15}	5.2×10^{11}	3340
	GaAs	1.1×10^{15}	2.9×10^{11}	3930
	In _{0.2} Ga _{0.8} As	5.2×10^{14}	2.6×10^{11}	2000
	In _{0.3} Ga _{0.7} As	8.5×10^{14}	4.3×10^{11}	1980

(blue bars) in Figure 10. We also calculated the generation currents using EQE and AM0 spectral irradiance [24] and compared them with the I_{sc} values. However, the results show significant discrepancies (a few per cent for the InGaP cells and ~15% for the InGaAs cells), presumably because of the mismatch of spectral irradiance between the AM0 and our solar simulator. Therefore, we adopted the simple EQE integral for comparison.

According to the results shown in Figure 10, the InGaAs cells have less radiation resistance for the photogeneration currents. The difference in the I_{sc} resistance implies difficulties in radiation-hard designing when InGaAs cells are employed as bottom subcells in InGaP/GaAs/InGaAs IMM3J cells. The prospective remaining factors of the InGaAs subcell I_{sc} (green bars) are remarkably lower than that of the InGaP and GaAs subcells, implying a greater decrease in the minority-carrier diffusion length, which can be ascribed to the nature of the material. This phenomenon has been practically observed during the development of our IMM3J space solar cells. These results suggest that the radiation-hard cell designs of InGaAs bottom cells are extremely important for IMM3J space solar cells. Quantitative analysis of the degradation of the subcell I_{sc} in accordance with the particle fluence based on the EQE data is underway to obtain further information for IMM3J cell designing.

4.3. Open-circuit voltage degradation

V_{oc} is expressed by the following equation:

$$V_{OC} = \frac{nkT}{q} \ln \left(\frac{I_{SC}}{I_0} + 1 \right) \quad (2)$$

where q is the elementary charge, T is the temperature, and k is the Boltzmann constant. The I_{sc} , n , and I_0 values can be obtained from LIV and DIV. Therefore, the expected

remaining factors of V_{oc} can be calculated using the three experimental values before and after irradiation. In this study, we selected the same cells that were used for the I_{sc} analysis in the previous clause and compared the remaining factors of the experimental and calculated V_{oc} values. The results are represented as bar graphs in Figure 11, and the values of n and I_0 used in the V_{oc} calculation are presented in Table IV and were obtained from the fitting of the DIV characteristics.

The calculated V_{oc} remaining factors of the InGaAs cells shown in Figure 11 are lower than the experimentally obtained ones, which is in contrast to the tendency observed for the InGaP and GaAs cells. The disagreement suggests that the influence of the radiation damage on the V_{oc} in InGaAs cells is different from that in the InGaP and GaAs cells. The parameters used in the V_{oc} calculation (I_{sc} , I_0 , and n) are obtained for a strong electric field in the p/n junction. However, the field is fairly negligible at the operating condition for V_{oc} . While this fact seems to have negligible impact on the InGaP and GaAs cells, Equation 2 may not be suited for the strongly degraded InGaAs cell. If radiation defects in InGaAs result in a less increase of the recombination rate at V_{oc} when compared with InGaP and GaAs, degradation of V_{oc} should be less than the theoretically predicted value.

The radiation resistance of V_{oc} for the InGaAs cells is comparable with that of the InGaP cells for both cases of electron and proton irradiations, which is clearly different from the radiation resistance of I_{sc} . The GaAs cells show rather low resistance, lower than any of the other three types of cells. As described in the ‘‘Degradation characteristics’’ clause, this fact most likely reflects the cell’s material quality; higher-quality cells generally indicate lower remaining factors. Because the two InGaAs cells were grown on lattice-mismatched GaAs substrates, the InGaAs layers contain a certain number of misfit dislocations. The existence of these misfit dislocations may positively affect the remaining factor of V_{oc} . However, this does not mean that the InGaAs cells used in this study have insufficient quality, because the initial V_{oc} of the InGaAs cells are equivalent to that of the InGaP cells (Table I).

Meanwhile, the 2D-PL images shown in Figure 8, where the observed PL is considered to originate from the surface region of the cells, indicate that after irradiation the InGaP and GaAs cells have suffered a significant decrease in PL intensity, whereas the two InGaAs cells show negligible changes. Possible causes for a decrease in PL intensity are increase of recombination at the window/emitter interface (surface recombination) and that in the emitter and top of the base layers (bulk recombination) of the cells. We consider that under laser excitation, a considerable number of photo-carriers are generated. Thus, the electric field in the space charge region should be as small as in the V_{oc} condition, and the recombination in the top of the base layers must be significant because the majority of the photo-generated carriers recombine in the p/n junction region. On the other hand, the EQE in the short-wavelength region of all four types of cells does not

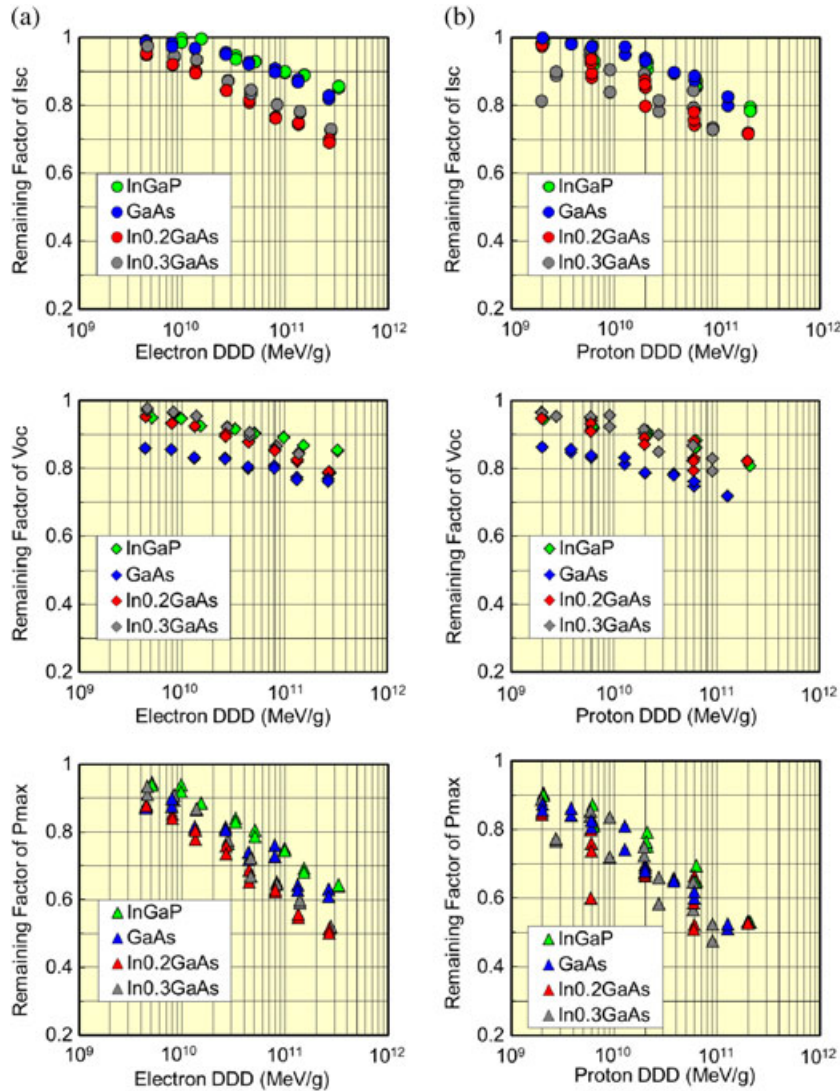


Figure 9. Degradation characteristics of I_{sc} , V_{oc} , and P_{max} as a function of the displacement damage dose (DDD). (a) Electrons and (b) protons.

Table III. Displacement damage dose values (MeV/g in unit) of 1 MeV electrons and 3 MeV protons with the fluences of 3×10^{15} and $3 \times 10^{12} \text{ cm}^{-2}$, respectively.

Cell	1 MeV electron, $3 \times 10^{15} \text{ cm}^{-2}$	3 MeV proton, $3 \times 10^{12} \text{ cm}^{-2}$
InGaP	9.9×10^{10}	6.2×10^{10}
GaAs	8.0×10^{10}	6.0×10^{10}
$\text{In}_{0.2}\text{Ga}_{0.8}\text{As}$	8.1×10^{10}	5.9×10^{10}
$\text{In}_{0.3}\text{Ga}_{0.7}\text{As}$	8.4×10^{10}	5.9×10^{10}

change with irradiation (Figures 4 and 5). This fact indicates that the surface recombination does not increase effectively because of irradiation, and the main reason for the change in PL intensity has to be the bulk recombination.

The InGaP and the two InGaAs cells show a relatively high remaining factor for V_{oc} . We presume this is

primarily because of their larger W_{oc} compared with the GaAs cells. However, we consider that the reason for this tendency is not the same for these two types of devices. Our experiments outlined above provided much information on the details of degradation. Many complex trends have been observed for the different cells. In the following, we report considerations for each solar cell type.

In the case of the InGaAs cells after irradiation, PL intensity was maintained but the EQE in the long-wavelength region dropped dramatically. Because the PL intensity does not decrease considerably by irradiation, an increase of the bulk recombination does not seem to be significant. This may be the reason of the higher remaining factor for the InGaAs cells. In addition, the stronger degradation of the effective minority-carrier diffusion length in the InGaAs cells shown in the EQE can be attributed to the increase in the back-surface recombination, which primarily causes the degradation of V_{oc} .

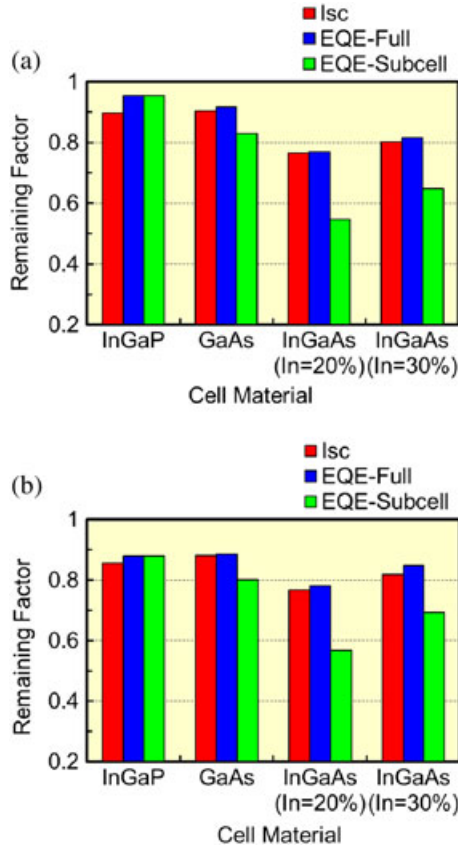


Figure 10. Average remaining factor values of I_{sc} and two integrated external quantum efficiency (EQE), full and subcell response wavelength region. (a) 1 MeV electron, fluences of $3 \times 10^{15} \text{ cm}^{-2}$ and (b) 3 MeV proton, fluences of $3 \times 10^{12} \text{ cm}^{-2}$.

In the case of the InGaP cells, PL intensity decreased noticeably but the reduction of EQE was relatively small. Therefore, a drastic increase of the bulk recombination by irradiation especially in the emitter layer is likely. However, the effective minority-carrier diffusion length of the InGaP cells is not affected by irradiation presumably because of less increase in back-surface recombination. This should be the reason of the higher V_{oc} remaining factor of the InGaP cells.

It is notable that in the case of the GaAs cells both the PL intensity and EQE significantly decreased because of irradiation. This is explained with the high initial material quality, leading to evident degradation in V_{oc} and also PL intensity.

The difference of the radiation effects might provide a clue to explain the different tendencies of the InGaAs cells observed in Figure 11, but we were not able to find a consistent explanation yet. To confirm the validity of the interpretation mentioned earlier, quantitative analysis of the V_{oc} and also I_{sc} degradation is necessary to gain deeper insights into the degradation characteristics of the four types of the cells. The analysis has to be carried out by extracting the surface and back-surface recombination velocities and the minority-carrier diffusion length from EQE. In

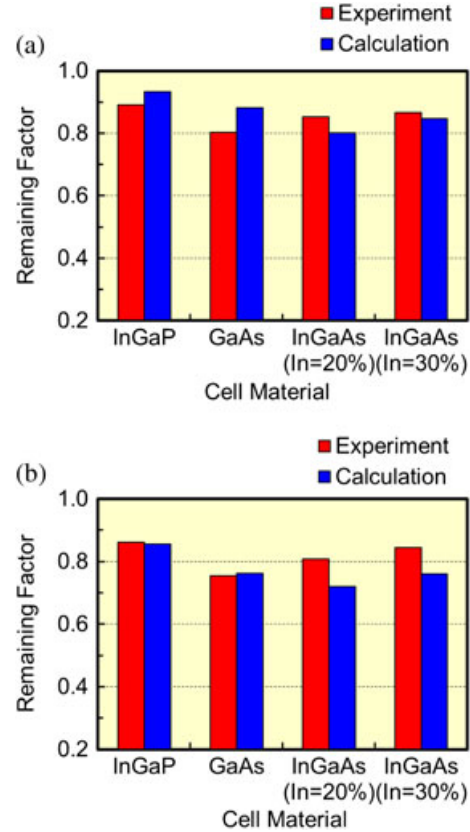


Figure 11. Average remaining factor values of experimental and calculated V_{oc} . (a) 1 MeV electron, fluences of $3 \times 10^{15} \text{ cm}^{-2}$ and (b) 3 MeV proton, fluences of $3 \times 10^{12} \text{ cm}^{-2}$.

Table IV. The best fit values of the diode factor n and the reverse saturation current I_0 values used in the calculation for Figure 11.

Irradiation Parameter	1 MeV electron, $3 \times 10^{15} \text{ cm}^{-2}$		3 MeV proton, $3 \times 10^{12} \text{ cm}^{-2}$		
	n	I_0	n	I_0	
InGaP	Initial	2.0	5.0×10^{-15}	2.1	2.0×10^{-14}
	Irradiated	2.0	3.0×10^{-14}	2.1	5.0×10^{-13}
GaAs	Initial	2.5	2.0×10^{-10}	2.2	1.0×10^{-10}
	Irradiated	2.6	3.0×10^{-9}	2.0	2.0×10^{-9}
$\text{In}_{0.2}\text{Ga}_{0.8}\text{As}$	Initial	2.2	2.5×10^{-8}	2.2	2.5×10^{-8}
	Irradiated	2.1	1.8×10^{-7}	2.1	6.0×10^{-7}
$\text{In}_{0.3}\text{Ga}_{0.7}\text{As}$	Initial	1.8	6.0×10^{-8}	2.1	3.0×10^{-7}
	Irradiated	1.9	6.5×10^{-7}	2.0	2.5×10^{-6}

They are obtained from the DIV fitting.

addition, we need to obtain the n_1/n_2 and I_{01}/I_{02} values by applying a two-diode model fitting of the DIV data. Moreover, we require a thorough understanding of what the PL intensity represents by considering the cell structures. We have proposed advanced analysis of solar cell operation using electroluminescence and time-resolved

PL characteristics [25,26], and our preliminary results have indicated that the luminescence efficiency of the InGaP cell under AM0, 1 sun illumination is not as high as we have expected from the relatively good cell performance [25]. The reason for this is under investigation, but might explain the similarity with the InGaAs cells. A similar analysis on the four types of 1J cells are underway and results will be published elsewhere together with the results of the analysis on I_{sc} . Further, analysis on radiation defect characteristics should help to let us understand the radiation response of the 1J solar cells. The observed degradation characteristics are important information to consider future designs of InGaP/GaAs/InGaAs IMM3J space cells.

5. CONCLUSIONS

This study analyzes the radiation response of simple structure $\text{In}_{0.5}\text{Ga}_{0.5}\text{P}$, GaAs, $\text{In}_{0.2}\text{Ga}_{0.8}\text{As}$, and $\text{In}_{0.3}\text{Ga}_{0.7}\text{As}$ 1J cells, which are the component subcell materials in present IMM3J cell designs. The four types of cells were irradiated with high-energy electrons and protons. The degradation tendencies of I_{sc} , V_{oc} , and P_{max} for the four types of cells were compared and analyzed using LIV and DIV characteristics, together with the EQE and 2D-PL images before and after the irradiations. A systematic comparison of the degradation tendencies of the three output parameters using the DDD analysis suggests that radiation resistance of the InGaAs cells is not always least among the three subcells from the materials standpoint. However, the radiation resistance of InGaAs cells is lower for I_{sc} . This can be attributed to the stronger decrease of minority-carrier diffusion length in InGaAs compared with that in InGaP and GaAs. This causes severe radiation degradation of photo-generation current in the InGaAs bottom subcell of InGaP/GaAs/InGaAs IMM3J cells. On the other hand, the radiation resistance of V_{oc} of the InGaAs cells is comparable with that of the InGaP cells, despite their lower bandgap. Further analytical studies are necessary to find out the reason of the characteristic radiation response of the subcells. However, we believe that the results obtained in this study are important and will contribute to the improvement of the radiation resistance of IMM3J space solar cells.

ACKNOWLEDGEMENTS

We would like to express our sincere thanks to Mr. T. Osada of Sumitomo Chemical Co. Ltd. and Mr. H. Washio of SHARP Corporation for their support in preparing the solar cells for analysis. Special thanks to Dr. S. Sato and Mr. H. Abe of Japan Atomic Energy Agency for their assistance in conducting the irradiation tests, Mr. G. Kato of Meiji University for his assistance in performing the photoluminescence experiment, and Mrs. J. Harada and M. Sugai of AES Corporation for assisting in solar cell

characterization measurement. We sincerely appreciate the insightful discussion with Prof. S. Messenger of the University of Maryland.

REFERENCES

1. Patel P, Aiken D, Boca A, Cho B, Chumney D, Clevenger MB, Cornfeld A, Fatemi N, Lin Y, McCarty J, Newman F, Sharps P, Spann J, Stan M, Steinfeldt J, Strautin C, Varghese T. Experimental results from performance improvement and radiation hardening of inverted metamorphic multijunction solar cells. *IEEE Journal of Photovoltaics* 2012; **2**: 377–381.
2. Boisvert J, Law D, King R, Rehder E, Chiu P, Bhusari D, Fetzer C, Liu X, Hong W, Mesropian S, Woo R, Edmondson K, Cotal H, Krut D, Singer S, Wierman S, Karam NH. High efficiency Inverted Metamorphic (IMM) solar cells, Proceedings of 39th IEEE Photovoltaic Specialists Conference 2013: 2790–2792.
3. Takamoto T, Washio H, Juso H. Application of InGaP/GaAs/InGaAs triple junction solar cells to space use and concentrator photovoltaic, Proceedings of 40th IEEE Photovoltaic Specialists Conference 2014: 1–5.
4. Tatavarti R, Wibowo A, Elarde V, Tuminello F, Pastor R, Giannopoulos T, Osowski M, Chan R, Youtsey C, Hillier G, Pan N. Large-area, epitaxial lift-off, inverted metamorphic solar cells, Proceedings of 37th IEEE Photovoltaic Specialists Conference 2011: 1941–1944.
5. France RM, Geisz JF, Steiner MA, Friedman DJ, Ward JS, Olson JM, Olavarria W, Young M, Duda A. Pushing inverted metamorphic multijunction solar cells toward higher efficiency at realistic operating conditions. *IEEE Journal of Photovoltaics* 2013; **3**: 893–898.
6. Jun B, Fetzer CM, Rouhani K, Wise WG, Krut D, Kiem B, Hom D, Cho CJ, Wu JZ, Anaya R, Bardfield R, Russell DA, Leung P, Gillanders M, Sharma SK, Hanley JP. Final qualification test results of XTJ triple junction space solar cell to AIAA-S-111-2005 and Spectrolab test standards, Proceedings of 35th IEEE Photovoltaic Specialists Conference 2010: 2554–2559.
7. Fatemi N, Lyons J, Eskenazi M. Qualification and production of Emcore ZTJ solar panels for space missions, Proceedings of 39th IEEE Photovoltaic Specialists Conference 2013: 2793–2796.
8. Yamaguchi H, Takahashi N, Kodama T, Izichi R, Washio H, Nakamura K, Takamoto T, Imaizumi M, Takahashi M, Shimazaki K, Kibe K. Development status of “Space Solar Sheet,” Proceedings of 33rd IEEE Photovoltaic Specialists Conference 2008: 1–3.
9. Miyamoto H, Chan R, Stender C, Youtsey C, Elarde V, Adams J, Tatavarti R, Osowski M, Pan N. Flexible,

- high specific power triple junction solar cell sheets and applications, Proceedings of 6th World Conference on Photovoltaic Energy Conversion 2014: 749–750.
10. Chumney D, Aiken D, Cho B, Cornfeld A, Diaz J, Ley V, Mittman J, Newman F, Sharps P, Stan M, Varghese T. Path to a drop-in replacement for current technologies with the 33%, large area, IMM cell, Proceedings of 35th IEEE Photovoltaic Specialists Conference 2010: 113–116.
 11. for example Yamaguchi M, Ando K. Mechanism for radiation resistance of InP solar cells. *Journal of Applied Physics* 1988; **63**: 5555–5562 b Dharmarasu N, Khan A, Yamaguchi M, Takamoto T, Ohshima T, Itoh H, Imaizumi M, Matsuda S. Effects of proton irradiation on n+p InGaP solar cells. *Journal of Applied Physics* 2002; **91**: 3306–3311.
 12. Walters RJ, Messenger SR, Summers GP, Bett AW, Dimroth F, Hoffman RW, Stan MA Jr., Takamoto T, Ikeda E, Imaizumi M, Anzawa O, Matsuda S. Radiation response of Ga_xIn_{1-x}As solar cells, Proceedings of 16th European Photovoltaic Solar Energy Conference 2000: 1030–1033.
 13. Imaizumi M, Takamoto T, Sumita T, Ohshima T, Yamaguchi M, Matsuda S, Ohi A, Kamiya T. Study of radiation response on single-junction component sub-cells in triple-junction solar cells, Proceedings of 3rd World Conference on Photovoltaic Energy Conversion 2003: CD 3OD602.
 14. Wanlass MW, Ahrenkiel SP, Ahrenkiel RK, Albin DS, Carapella JJ, Duda A, Geisz JF, Kurtz S, Moriarty T, Wehrer RJ, Wernsman B. Lattice-mismatched approaches for high-performance, III-V photovoltaic energy converters, Proceedings of 31st IEEE Photovoltaic Specialists Conference 2005: 530–535.
 15. Takamoto T, Agui T, Yoshida A, Nakaido K, Juso H, Sasaki K, Nakamura K, Yamaguchi H, Kodama T, Washio H, Imaizumi M, Takahashi M. World's highest efficiency triple-junction solar cells fabricated by inverted layers transfer process, Proceedings of 35th IEEE Photovoltaic Specialists Conference 2010: 412–417.
 16. ISO15387. *Space Systems—Single-junction Solar Cells—Measurements and Calibration Procedures*. International Organization for Standardization: Geneva, 2005.
 17. Tajima M, Li Z, Shimidzu R. Photoluminescence mapping system applicable to 300 mm silicon-on-insulator wafers. *Japanese Journal of Applied Physics* 2002; **41**: L1505–L1507.
 18. Ziegler JF, Biersack JP, Ziegler D. SRIM The Stopping and Range of Ions in Matter, see <http://www.srim.org/> n.d.
 19. JAEA Takasaki, see http://www.taka.jaea.go.jp/tiara/index_e.htm n.d.
 20. Tada HY, Carter JR Jr, Anspaugh BE, Downing RG. *Solar Cell Radiation Handbook 82-69*. JPL Publication: Pasadena, 1982. 3-17–3-20.
 21. Imaizumi M, Taylor SJ, Yamaguchi M, Ito T, Hisamatsu T, Matsuda S. Analysis of structure change of Si solar cells irradiated with high fluence electrons. *Journal of Applied Physics* 1999; **85**: 1916–1920.
 22. Summers GP, Walters RJ, Xapsos MA, Bruke EA, Messenger SR, Shapiro P, Statler RL. A new approach to damage prediction for solar cells exposed to different radiations, Proceedings of 1st World Conference on Photovoltaic Energy Conversion 1994: 2068–2075.
 23. Messenger SR, Summers GP, Bruke EA, Walters RJ, Xapsos MA. Modeling solar cell degradation in space: a comparison of the NRL displacement damage dose and the JPL equivalent fluence approaches. *Progress in Photovoltaics: Research and Applications* 1997; **44**: 103–121.
 24. ASTM, E490-00a. *Standard Solar Constant and Zero Air Mass Solar Spectral Irradiance Tables*. ASTM International: West Conshohocken, 2014.
 25. Zhu L, Yoshita M, Chen S, Nakamura T, Mochizuki T, Kim C, Imaizumi M, Kanemitsu Y, Akiyama H. Characterizations of radiation damages in multi-junction solar cells focused on subcell internal luminescence quantum yields via absolute electroluminescence measurements. *IEEE Journal of Photovoltaics* 2016; **6**: 777–782.
 26. Tex DM, Nakamura T, Imaizumi M, Ohshima T, Kanemitsu Y. Direct Evaluation of influence of electron damage on the subcell operating voltage and current in triple-junction solar cells using photoluminescence decays: progress in photovoltaics: research and applications; submitted (PIP-16-081) n.d.